Available online at www.sciencedirect.com
SCIENCE DIRECT
Computers and Structures 84 (2006) 1275–1287
Computers & Structures
www.elsevier.com/locate/compstruc

Geometrically exact assumed stress–strain multilayered solid-shell elements based on the 3D analytical integration

G.M. Kulikov *, S.V. Plotnikova

Department of Applied Mathematics and Mechanics, Tambov State Technical University, Sovetskaya Street 106, 392000 Tambov, Russia

Received 16 June 2005; accepted 16 January 2006
Available online 19 May 2006

Abstract

This paper presents a family of geometrically exact assumed stress–strain four-node curved solid-shell elements with six displacement degrees of freedom per node by using the first-order equivalent single-layer theory. The proposed finite element formulation is based on the new strain–displacement relationships written in general reference surface coordinates, which are objective, i.e., invariant under rigid-body motions. This is possible because displacement vectors of the bottom and top surfaces of the shell are introduced and resolved in the reference surface frame. To overcome shear and membrane locking and have no spurious zero energy modes, the assumed strain and stress resultant fields are invoked. In order to circumvent thickness locking, three types of the modified material stiffness matrix extracted from the literature are employed and compared. All three elemental stiffness matrices have six zero eigenvalues and require only direct substitutions. Besides, they are evaluated by applying the 3D analytical integration that is very economical and allows using extremely coarse meshes.

Keywords: First-order shell theory; Assumed stress–strain element; Analytical integration

1. Introduction

In the last 15 years, a considerable work has been carried out on three-dimensional continuum-based finite elements that can handle shell analysis satisfactorily. These elements are typically defined by two layers of nodes at the bottom and top surfaces of the shell with three displacement degrees of freedom per node and known as *isoparametric* solid-shell elements [1–10]. In the isoparametric solid-shell element formulation, initial and deformed geometry are equally interpolated allowing one to describe rigid-body motions precisely. The development of solid-shell elements is not straightforward. In order to overcome element deficiencies such as shear, membrane, trapezoidal and thickness locking, advanced finite element techniques including assumed natural strain, assumed strain, enhanced assumed strain and hybrid stress methods have to be applied. Still, the isoparametric solid-shell element formulation is computationally inefficient because stresses and strains are analyzed in the global or local orthogonal Cartesian coordinate system, although the normalized element coordinates represent already curvilinear convective coordinates.

An alternative way is to develop the *geometrically exact* solid-shell element based on the *general* curvilinear coordinates that finds its point of departure in papers [11–15], in which only orthogonal curvilinear reference surface coordinates were employed. The term ''geometrically exact'' reflects the fact that reference surface geometry is described by analytically given functions. Such elements are very promising due to the fact that in the geometric modeling of modern CAD systems the surfaces are usually generated by non-uniform rational B-splines (NURBS) [16]. Allowing for that surfaces are conventionally produced by the position vector with representation of two parameters, we can connect the geometric modeling of the shell surface generated in the CAD system to the finite element analysis

* Corresponding author. Fax: +7 475 271 0216.
E-mail addresses: kulikov@apmath.tstu.ru, gmkulikov@mail.ru (G.M. Kulikov).

0045-7949/$ - see front matter
doi:10.1016/j.compstruc.2006.01.034

of shell structures. So, it is advantageous to use NURBS shell surface functions directly in the shell calculations and geometrically exact solid-shell elements are best suited for this purpose. They also have the two-parameter representation in surfaces and all geometric computations may be done in the reference surface using NURBS surface representations in the CAD system.

The solid-shell element formulation developed is based on the principally new strain–displacement relationships of the first-order equivalent single-layer (ESL) theory, written in the general reference surface coordinates. It is remarkable that these strain–displacement relationships *precisely* represent all rigid-body motions and no assumptions except for standard Timoshenko–Mindlin kinematics are required to derive them. For this purpose displacement vectors of the bottom and top surfaces of the shell are introduced but resolved, in contrast with the isoparametric solid-shell formulation [1–10], in the reference surface frame. One can compare the proposed shell formulation with a close formulation of Simo et al. [17], where geometrically exact solid-shell elements have been also developed but displacement vectors are resolved in the global Cartesian basis and, therefore, Christoffel symbols and coefficients of the second fundamental form do not explicitly appear in the formulation. This restriction does not give an opportunity to employ the above NURBS surface function technique directly.

The finite element formulation is based on the simple and efficient approximation of shells via four-node curved shell elements. To avoid shear and membrane locking and have no spurious zero energy modes, the assumed stress resultant and displacement-independent strain fields are invoked. This approach was proposed by Wempner et al. [18] for the classic first-order shear deformation shell theory and further was generalized by Kulikov and Plotnikova [14,15] for the so-called Timoshenko–Mindlin shell theory allowing for the thickness change.

It is known that a six-parameter shell formulation on the basis of the complete 3D constitutive equations is deficient because thickness locking can occur [10]. To prevent thickness locking at the *finite element level* an efficient enhanced assumed strain method [3,4] can be applied. In order to circumvent a locking phenomenon at the *mechanical level* and computational one as well, the 3D constitutive equations have to be modified. For this purpose three simple and effective remedies may be employed, namely, the *ad-hoc* modified laminate stiffness matrix [9,19,20] and simplified material stiffness matrices symmetric [1,2,6,14,21] or non-symmetric [15,22,23] corresponding to the generalized plane stress condition. Herein, all remedies are introduced into the formulation that allows one to assess their advantages and disadvantages.

Taking into account that displacement vectors of bottom and top surfaces of the shell are represented in the reference surface frame, the proposed geometrically exact solid-shell formulations have computational advantages compared to the conventional isoparametric finite element formulations, since they reduce the costly numerical integration by deriving the stiffness matrices. Besides, element matrices developed require only direct substitutions, i.e., no inversion is needed if sides of the element coincide with lines of principal curvatures of the reference surface and they are evaluated by using the 3D analytical integration. As it turned out, an analytical integration leading to the elemental stiffness matrix is very economical and performs well even for the extremely coarse meshes.

2. Geometry and kinematic description of shell

Consider a shell built up in the general case by the arbitrary superposition across the wall thickness of N layers of uniform thickness h_k. The kth layer may be defined as a 3D body of volume V_k bounded by two surfaces S_{k-1} and S_k, located at the distances δ_{k-1} and δ_k measured with respect to the reference surface S, and the edge boundary surface Ω_k (Fig. 1). The full edge boundary surface $\Omega = \Omega_1 + \Omega_2 + \cdots + \Omega_N$ is generated by the normals to the reference surface along the bounding curve $\Gamma \subset S$. It is also assumed that the bounding surfaces S_{k-1} and S_k are continuous, sufficiently smooth and without any singularities. Let the reference surface S be referred to the general curvilinear coordinate system α^1 and α^2. The coordinate α^3 is oriented along the unit vector $\boldsymbol{a}_3$ normal to the reference surface, while $\boldsymbol{a}_1$ and $\boldsymbol{a}_2$ denote the covariant basis vectors of the reference surface.

The constituent layers of the shell are supposed to be rigidly joined, so that no slip on contact surfaces and no separation of layers can occur. The material of each con-

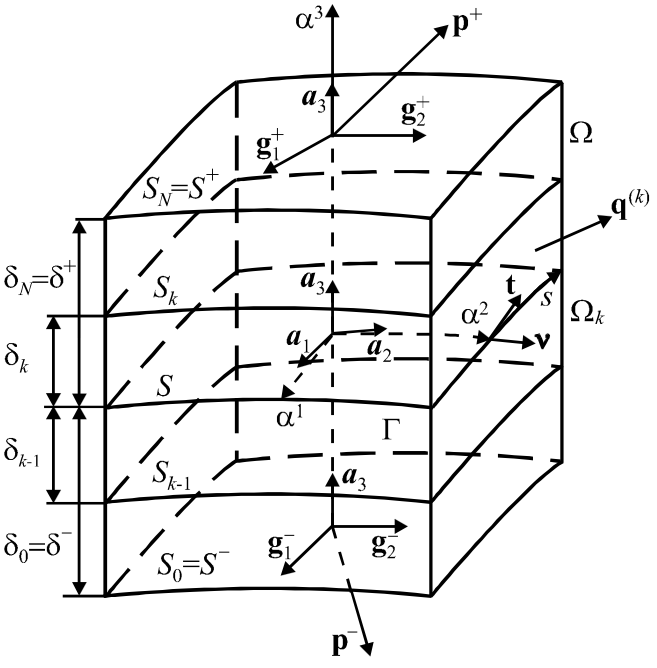

Fig. 1. Multilayered shell.

stituent layer is assumed to be linearly elastic, anisotropic, homogeneous or fiber reinforced, such that in each point there is a single surface of elastic symmetry parallel to the reference surface. Let $\mathbf{p}^-$ and $\mathbf{p}^+$ be the external loading vectors acting on the bottom surface $S^- = S_0$ and top surface $S^+ = S_N$; $\mathbf{q}^{(k)} = q_\nu^{(k)}\boldsymbol{\nu} + q_t^{(k)}\mathbf{t} + q_3^{(k)}\boldsymbol{a}_3$ be the external loading vector acting on the edge boundary surface Ω_k, where $q_\nu^{(k)}$, $q_t^{(k)}$ and $q_3^{(k)}$ are the components of its vector in the ν, t and α^3 directions; $\boldsymbol{\nu}$ and $\mathbf{t}$ denote the normal and tangential unit vectors to the bounding curve Γ. Here and in the following developments the index k identifies the belonging of any quantity to the kth layer and runs from 1 to N; the abbreviation $(\,)_{,\alpha}$ implies the partial derivatives with respect to coordinates α^1 and α^2; indices i, j, ℓ, m take the values 1, 2 and 3 while Greek indices $\alpha, \beta, \gamma, \delta$ take the values 1 and 2.

The position vector $\mathbf{R}$ of the arbitrary point in the shell body can be expressed as

$$\mathbf{R} = N^-\mathbf{R}^- + N^+\mathbf{R}^+, \quad \mathbf{R}^\pm = \mathbf{r} + \delta^\pm \boldsymbol{a}_3, \tag{1a}$$

$$N^- = \frac{1}{h}(\delta^+ - \alpha^3), \quad N^+ = \frac{1}{h}(\alpha^3 - \delta^-), \tag{1b}$$

where $\mathbf{r}(\alpha^1, \alpha^2)$ is the position vector of the reference surface; $\mathbf{R}^\pm$ are the position vectors of the face surfaces; $N^\pm(\alpha^3)$ are the linear through-thickness shape functions of the shell; h is the thickness of the shell.

The covariant base vectors of the arbitrary point of the shell are derived by partial differentiating position vectors (1a)

$$\begin{aligned} &\mathbf{g}_\alpha = \mathbf{R}_{,\alpha} = N^-\mathbf{g}_\alpha^- + N^+\mathbf{g}_\alpha^+, \quad \mathbf{g}_\alpha^\pm = \mathbf{R}_{,\alpha}^\pm = \zeta_\alpha^{\pm\beta}\boldsymbol{a}_\beta, \\ &\mathbf{g}_3 = \mathbf{g}_3^\pm = \boldsymbol{a}_3, \quad \boldsymbol{a}_\alpha = \mathbf{r}_{,\alpha}, \\ &\zeta_\alpha^{\pm\beta} = \delta_\alpha^\beta - b_\alpha^\beta\delta^\pm, \quad b_\alpha^\beta = -\boldsymbol{a}^\beta \cdot \boldsymbol{a}_{3,\alpha}, \end{aligned} \tag{2}$$

where $\boldsymbol{a}^i$ are the contravariant base vectors of the reference surface defined by the standard relation $\boldsymbol{a}_i \cdot \boldsymbol{a}^j = \delta_i^j$ and b_α^β are the mixed components of the curvature tensor. The covariant base vectors of the middle surface are given by

$$\begin{aligned} &\mathbf{g}_\alpha^{\mathrm{M}} = \frac{1}{2}(\mathbf{g}_\alpha^- + \mathbf{g}_\alpha^+) = \zeta_\alpha^{\mathrm{M}\beta}\boldsymbol{a}_\beta, \quad \mathbf{g}_3^{\mathrm{M}} = \boldsymbol{a}_3, \\ &\zeta_\alpha^{\mathrm{M}\beta} = \frac{1}{2}(\zeta_\alpha^{-\beta} + \zeta_\alpha^{+\beta}) = \delta_\alpha^\beta - b_\alpha^\beta\delta^{\mathrm{M}}, \quad \delta^{\mathrm{M}} = \frac{1}{2}(\delta^- + \delta^+), \end{aligned} \tag{3}$$

where δ^{M} is the distance from the reference surface to the middle surface.

The ESL shell theory is based on the linear approximation of displacements in the thickness direction (Timoshenko–Mindlin kinematics)

$$\hat{\mathbf{R}} = N^-\hat{\mathbf{R}}^- + N^+\hat{\mathbf{R}}^+, \quad \hat{\mathbf{R}}^\pm = \mathbf{R}^\pm + \mathbf{u}^\pm, \tag{4}$$

where $\hat{\mathbf{R}}$ and $\hat{\mathbf{R}}^\pm$ are the position vectors of points in the shell body in its current configuration (Fig. 2); $\mathbf{u}^\pm(\alpha^1, \alpha^2)$ are the displacement vectors of the face surfaces defined as

$$\mathbf{u}^\pm = u_i^\pm \boldsymbol{a}^i. \tag{5}$$

It should be remarked that displacement vectors (5) are resolved in the dual reference surface basis $\boldsymbol{a}^i$ that allows one to reduce the costly numerical integration by evaluating the stiffness matrix.

The covariant base vectors in the current shell configuration are derived by partial differentiating position vectors (4)

$$\hat{\mathbf{g}}_\alpha = \hat{\mathbf{R}}_{,\alpha} = N^-\hat{\mathbf{g}}_\alpha^- + N^+\hat{\mathbf{g}}_\alpha^+, \quad \hat{\mathbf{g}}_\alpha^\pm = \hat{\mathbf{R}}_{,\alpha}^\pm = \mathbf{g}_\alpha^\pm + \boldsymbol{u}_{,\alpha}^\pm, \tag{6a}$$

$$\begin{aligned} &\hat{\mathbf{g}}_\alpha^{\mathrm{M}} = \frac{1}{2}(\hat{\mathbf{g}}_\alpha^- + \hat{\mathbf{g}}_\alpha^+) = \mathbf{g}_\alpha^{\mathrm{M}} + \mathbf{u}_{,\alpha}^{\mathrm{M}}, \quad \hat{\mathbf{g}}_3 = \hat{\mathbf{g}}_3^\pm = \hat{\mathbf{g}}_3^{\mathrm{M}} = \hat{\boldsymbol{a}}_3, \\ &\hat{\boldsymbol{a}}_3 = \boldsymbol{a}_3 + \boldsymbol{\beta}, \\ &\mathbf{u}^{\mathrm{M}} = \frac{1}{2}(\mathbf{u}^- + \mathbf{u}^+), \quad \boldsymbol{\beta} = \frac{1}{h}(\mathbf{u}^+ - \mathbf{u}^-), \end{aligned} \tag{6b}$$

where $\mathbf{u}^{\mathrm{M}}$ is the displacement vector of the middle surface.

3. Strain–displacement relationships

The components of the Green–Lagrange (GL) strain tensor can be written as

$$2\varepsilon_{ij}^{\mathrm{GL}} = \hat{\mathbf{g}}_i \cdot \hat{\mathbf{g}}_j - \mathbf{g}_i \cdot \mathbf{g}_j. \tag{7}$$

Substituting covariant base vectors in the reference and current shell configurations (2) and (6a) into the 3D strain–displacement relationships (7), the following strain–displacement relationships of the ESL shell theory are obtained:

$$\varepsilon_{\alpha\beta}^{\mathrm{GL}} = L^-\mathscr{E}_{\alpha\beta}^- + L^{\mathrm{M}}\mathscr{E}_{\alpha\beta}^{\mathrm{M}} + L^+\mathscr{E}_{\alpha\beta}^+, \tag{8a}$$

$$\varepsilon_{\alpha3}^{\mathrm{GL}} = N^-\mathscr{E}_{\alpha3}^- + N^+\mathscr{E}_{\alpha3}^+, \quad \varepsilon_{33}^{\mathrm{GL}} = \mathscr{E}_{33}, \tag{8b}$$

$$\begin{aligned} &L^- = N^-(N^- - N^+), \quad L^{\mathrm{M}} = 4N^-N^+, \\ &L^+ = N^+(N^+ - N^-), \end{aligned} \tag{8c}$$

where $L^\pm(\alpha^3)$ and $L^{\mathrm{M}}(\alpha^3)$ are the quadratic through-thickness shape functions of the shell; $\mathscr{E}_{\alpha\beta}^\pm$ and $\mathscr{E}_{\alpha\beta}^{\mathrm{M}}$ are the in-plane strains of face and middle surfaces, correspondingly; $\mathscr{E}_{\alpha3}^\pm$ are the transverse shear strains of face surfaces defined as

$$2\mathscr{E}_{\alpha\beta}^{\mathrm{I}} = \hat{\mathbf{g}}_\alpha^{\mathrm{I}} \cdot \hat{\mathbf{g}}_\beta^{\mathrm{I}} - \mathbf{g}_\alpha^{\mathrm{I}} \cdot \mathbf{g}_\beta^{\mathrm{I}} \quad (\mathrm{I} = -, \mathrm{M}, +), \tag{9a}$$

$$2\mathscr{E}_{\alpha3}^\pm = \hat{\mathbf{g}}_\alpha^\pm \cdot \hat{\boldsymbol{a}}_3 - \mathbf{g}_\alpha^\pm \cdot \boldsymbol{a}_3, \quad 2\mathscr{E}_{33} = \hat{\boldsymbol{a}}_3 \cdot \hat{\boldsymbol{a}}_3 - \boldsymbol{a}_3 \cdot \boldsymbol{a}_3. \tag{9b}$$

The strain terms (8a) quadratic in α^3 can be neglected because of their minor significance in most ESL shell formulations. So, we employ assumed Green–Lagrange (AGL) strains as follows:

$$\varepsilon_{\alpha\beta}^{\mathrm{AGL}} = N^-\mathscr{E}_{\alpha\beta}^- + N^+\mathscr{E}_{\alpha\beta}^+, \tag{10a}$$

$$\varepsilon_{\alpha3}^{\mathrm{AGL}} = N^-\mathscr{E}_{\alpha3}^- + N^+\mathscr{E}_{\alpha3}^+, \quad \varepsilon_{33}^{\mathrm{AGL}} = \mathscr{E}_{33}. \tag{10b}$$

Remark 1. The in-plane components of GL and AGL strain tensors satisfy the following linking conditions:

$$\varepsilon_{\alpha\beta}^{\mathrm{GL}}(\delta^\pm) = \varepsilon_{\alpha\beta}^{\mathrm{AGL}}(\delta^\pm). \tag{11}$$

These conditions immediately follow from Eqs. (8a) and (10a) accounting for (1b) and (8c).

Proposition 1. *The GL strains of the proposed ESL theory are invariant under large rigid-body motions.*

Proof. An arbitrarily large rigid-body motion can be defined by

$$(\mathbf{u})^{\mathrm{Rigid}} = \boldsymbol{\Delta} + (\boldsymbol{\Phi} - \mathbf{I})\mathbf{R},$$

where $\boldsymbol{\Delta} = \Delta_i \boldsymbol{a}^i$ is the constant displacement (translation) vector; $\mathbf{I}$ is the identity matrix; $\boldsymbol{\Phi}$ is the orthogonal rotation matrix [24].

It is apparent that

$$\left(\hat{\mathbf{g}}^{\mathrm{I}}_{\alpha}\right)^{\mathrm{Rigid}} = \boldsymbol{\Phi}\mathbf{g}^{\mathrm{I}}_{\alpha} \ (\mathrm{I} = -, \mathrm{M}, +), \quad (\hat{\boldsymbol{a}}_3)^{\mathrm{Rigid}} = \boldsymbol{\Phi}\boldsymbol{a}_3. \tag{12}$$

It can be shown by using (12) that strains (9) are all zero in a general large rigid-body motion

$$\begin{aligned} 2(\mathscr{E}^{\mathrm{I}}_{\alpha\beta})^{\mathrm{Rigid}} &= \left(\boldsymbol{\Phi}\mathbf{g}^{\mathrm{I}}_{\alpha}\right)\cdot\left(\boldsymbol{\Phi}\mathbf{g}^{\mathrm{I}}_{\beta}\right) - \mathbf{g}^{\mathrm{I}}_{\alpha}\cdot\mathbf{g}^{\mathrm{I}}_{\beta} = 0 \quad (\mathrm{I} = -, \mathrm{M}, +),\\ 2(\mathscr{E}^{\pm}_{\alpha 3})^{\mathrm{Rigid}} &= (\boldsymbol{\Phi}\mathbf{g}^{\pm}_{\alpha})\cdot(\boldsymbol{\Phi}\boldsymbol{a}_3) - \mathbf{g}^{\pm}_{\alpha}\cdot\boldsymbol{a}_3 = 0,\\ 2(\mathscr{E}_{33})^{\mathrm{Rigid}} &= (\boldsymbol{\Phi}\boldsymbol{a}_3)\cdot(\boldsymbol{\Phi}\boldsymbol{a}_3) - \boldsymbol{a}_3\cdot\boldsymbol{a}_3 = 0. \end{aligned} \tag{13}$$

This conclusion is true because an orthogonal transformation retains the scalar product of the vectors. So, due to relations (13) GL strains (8) exactly represent arbitrarily large rigid-body motions, i.e.,

$$\left(\varepsilon^{\mathrm{GL}}_{ij}\right)^{\mathrm{Rigid}} = 0. \qquad \square$$

Proposition 2. *The AGL strains of the proposed ESL theory are invariant under large rigid-body motions.*

Proof. Using relations (13) into AGL strains (10) leads to the required result

$$\left(\varepsilon^{\mathrm{AGL}}_{ij}\right)^{\mathrm{Rigid}} = 0. \qquad \square$$

Further we represent strain–displacement relationships (9) by using Eq. (6) in the more convenient form

$$2\mathscr{E}^{\pm}_{\alpha\beta} = \mathbf{u}^{\pm}_{,\alpha}\cdot\mathbf{g}^{\pm}_{\beta} + \mathbf{u}^{\pm}_{,\beta}\cdot\mathbf{g}^{\pm}_{\alpha} + \mathbf{u}^{\pm}_{,\alpha}\cdot\mathbf{u}^{\pm}_{,\beta}, \tag{14a}$$

$$2\mathscr{E}^{\pm}_{\alpha 3} = \boldsymbol{\beta}\cdot\mathbf{g}^{\pm}_{\alpha} + \mathbf{u}^{\pm}_{,\alpha}\cdot(\boldsymbol{a}_3 + \boldsymbol{\beta}), \quad 2\mathscr{E}_{33} = \boldsymbol{\beta}\cdot(2\boldsymbol{a}_3 + \boldsymbol{\beta}), \tag{14b}$$

$$\mathbf{u}^{\pm}_{,\alpha} = (u^{\pm}_{i,\alpha} - \Gamma^{j}_{i\alpha}u^{\pm}_{j})\boldsymbol{a}^i, \tag{14c}$$

where $\Gamma^{j}_{i\alpha}$ are the Christoffel symbols defined by

$$\Gamma^{i}_{\alpha\beta} = \boldsymbol{a}^i\cdot\boldsymbol{a}_{\alpha,\beta}, \quad \Gamma^{\beta}_{3\alpha} = -b^{\beta}_{\alpha}, \quad \Gamma^{3}_{3\alpha} = 0. \tag{15}$$

Remark 2. The transverse components of the developed GL and AGL strain tensors satisfy the following coupling conditions:

$$2\left(\mathscr{E}^{+}_{\alpha 3} - \mathscr{E}^{-}_{\alpha 3}\right) = h\mathscr{E}_{33,\alpha}. \tag{16}$$

These conditions follow from Eqs. (2), (6b) and (14b)

$$\begin{aligned} 2\left(\mathscr{E}^{+}_{\alpha 3} - \mathscr{E}^{-}_{\alpha 3}\right) &= \boldsymbol{\beta}\cdot\left(\mathbf{g}^{+}_{\alpha} - \mathbf{g}^{-}_{\alpha}\right) + \left(\mathbf{u}^{+}_{,\alpha} - \mathbf{u}^{-}_{,\alpha}\right)\cdot(\boldsymbol{a}_3 + \boldsymbol{\beta})\\ &= h\left[-b^{\beta}_{\alpha}\boldsymbol{\beta}\cdot\boldsymbol{a}_{\beta} + \boldsymbol{\beta}_{,\alpha}\cdot(\boldsymbol{a}_3 + \boldsymbol{\beta})\right] = h\mathscr{E}_{33,\alpha}, \end{aligned}$$

and play a central role in our geometrically exact solid-shell elements.

If the reference surface S is referred to the orthogonal curvilinear coordinates, which coincide with lines of principal curvatures of its surface then

$$\begin{aligned} &\boldsymbol{a}_{\alpha} = A_{\alpha}\mathbf{e}_{\alpha}, \quad \boldsymbol{a}_3 = \mathbf{e}_3, \quad \mathbf{g}^{\pm}_{\alpha} = A_{\alpha}\zeta^{\pm}_{\alpha}\mathbf{e}_{\alpha}, \quad \zeta^{\pm}_{\alpha} = 1 + k_{\alpha}\delta^{\pm},\\ &b^1_1 = -k_1, \quad b^2_2 = -k_2, \quad b^2_1 = b^1_2 = 0. \end{aligned} \tag{17}$$

Using Eqs. (14) and (17) one derives the following strain–displacement relations:

$$2\overset{\circ}{\mathscr{E}}{}^{\pm}_{\alpha\beta} = \frac{\zeta^{\pm}_{\beta}}{A_{\alpha}}\mathbf{u}^{\pm}_{,\alpha}\cdot\mathbf{e}_{\beta} + \frac{\zeta^{\pm}_{\alpha}}{A_{\beta}}\mathbf{u}^{\pm}_{,\beta}\cdot\mathbf{e}_{\alpha} + \frac{1}{A_{\alpha}A_{\beta}}\mathbf{u}^{\pm}_{,\alpha}\cdot\mathbf{u}^{\pm}_{,\beta}, \tag{18a}$$

$$2\overset{\circ}{\mathscr{E}}{}^{\pm}_{\alpha 3} = \zeta^{\pm}_{\alpha}\boldsymbol{\beta}\cdot\mathbf{e}_{\alpha} + \frac{1}{A_{\alpha}}\mathbf{u}^{\pm}_{,\alpha}\cdot(\mathbf{e}_3 + \boldsymbol{\beta}), \quad 2\overset{\circ}{\mathscr{E}}{}_{33} = \boldsymbol{\beta}\cdot(2\mathbf{e}_3 + \boldsymbol{\beta}), \tag{18b}$$

where strains with a circle denote components of the AGL strain tensor in the orthonormal reference surface basis $\mathbf{e}_i$; A_{α} and k_{α} are the Lamé coefficients and principal curvatures of the reference surface.

Substituting displacements

$$\mathbf{u}^{\pm} = \sum_i v^{\pm}_i\mathbf{e}_i \tag{19}$$

into the linear strain–displacement relations (18) and computing Christoffel symbols (15) with account for formulas for the derivatives of unit vectors $\mathbf{e}_i$ with respect to the curvilinear coordinates α^1 and α^2, one can write these relations in a scalar form as

$$2\overset{\circ}{\mathscr{E}}{}^{\pm}_{\alpha\beta} = \zeta^{\pm}_{\alpha}\lambda^{\pm}_{\alpha\beta} + \zeta^{\pm}_{\beta}\lambda^{\pm}_{\beta\alpha}, \quad 2\overset{\circ}{\mathscr{E}}{}^{\pm}_{\alpha 3} = \zeta^{\pm}_{\alpha}\beta_{\alpha} - \theta^{\pm}_{\alpha}, \quad \overset{\circ}{\mathscr{E}}{}_{33} = \beta_3, \tag{20}$$

where

$$\begin{aligned} \lambda^{\pm}_{\alpha\alpha} &= \left(\frac{1}{A_{\alpha}}v^{\pm}_{\alpha}\right)_{,\alpha} + B_{\alpha\alpha}v^{\pm}_{\alpha} + B_{\alpha\beta}v^{\pm}_{\beta} + k_{\alpha}v^{\pm}_3 \quad (\beta \neq \alpha),\\ \lambda^{\pm}_{\beta\alpha} &= \left(\frac{1}{A_{\alpha}}v^{\pm}_{\beta}\right)_{,\alpha} + B_{\alpha\alpha}v^{\pm}_{\beta} - B_{\alpha\beta}v^{\pm}_{\alpha} \quad (\beta \neq \alpha),\\ \theta^{\pm}_{\alpha} &= -\left(\frac{1}{A_{\alpha}}v^{\pm}_3\right)_{,\alpha} - B_{\alpha\alpha}v^{\pm}_3 + k_{\alpha}v^{\pm}_{\alpha}, \quad \beta_i = \frac{1}{h}\left(v^{+}_i - v^{-}_i\right),\\ B_{\gamma\delta} &= \frac{1}{A_{\gamma}A_{\delta}}A_{\gamma,\delta}. \end{aligned} \tag{21}$$

Note that derivatives in Eq. (21) have been written in a form that is best suited for applying high performance analytical integration schemes inside the element.

4. Hu–Washizu variational equation

The first-order multilayered shell theory developed is based on the assumed approximations of displacements (4) and displacement-dependent strains (10) in the thickness direction. Additionally, one should adopt the similar approximation for the assumed displacement-independent strains

$$\varepsilon^{\mathrm{AS}}_{\alpha\beta} = N^{-}E^{-}_{\alpha\beta} + N^{+}E^{+}_{\alpha\beta}, \tag{22a}$$

$$\varepsilon^{\mathrm{AS}}_{\alpha 3} = N^{-}E^{-}_{\alpha 3} + N^{+}E^{+}_{\alpha 3}, \quad \varepsilon^{\mathrm{AS}}_{33} = E_{33}. \tag{22b}$$

Substituting approximations (4), (10) and (22) into the Hu–Washizu mixed variational principle [24] and accounting for that metrics of all surfaces parallel to the reference surface are identical and equal to the metric of the middle surface, one can derive

$$\int\int_{S} [(\mathbf{H} - \mathbf{DE})^{\mathrm{T}}\delta\mathbf{E} + (\mathbf{E} - \overset{\circ}{\boldsymbol{\mathscr{E}}})^{\mathrm{T}}\delta\mathbf{H} - \mathbf{H}^{\mathrm{T}}\delta\overset{\circ}{\boldsymbol{\mathscr{E}}} + \mathbf{P}^{\mathrm{T}}\delta\mathbf{v}] \times A^{\mathrm{M}}_1 A^{\mathrm{M}}_2 \,\mathrm{d}\alpha^1\,\mathrm{d}\alpha^2 + \oint_{\Gamma} \hat{\mathbf{H}}^{\mathrm{T}}_{\Gamma}\delta\mathbf{v}_{\Gamma}(1 + k_{\mathrm{N}}\delta^{\mathrm{M}})\,\mathrm{d}s = 0. \tag{23}$$

Here, matrix notations are introduced

$$\mathbf{D} = \begin{bmatrix}
D^{00}_{1111} & D^{01}_{1111} & D^{00}_{1122} & D^{01}_{1122} & D^{00}_{1112} & D^{01}_{1112} & 0 & 0 & 0 & 0 & D^{0}_{1133} \\
D^{01}_{1111} & D^{11}_{1111} & D^{01}_{1122} & D^{11}_{1122} & D^{01}_{1112} & D^{11}_{1112} & 0 & 0 & 0 & 0 & D^{1}_{1133} \\
D^{00}_{2211} & D^{01}_{2211} & D^{00}_{2222} & D^{01}_{2222} & D^{00}_{2212} & D^{01}_{2212} & 0 & 0 & 0 & 0 & D^{0}_{2233} \\
D^{01}_{2211} & D^{11}_{2211} & D^{01}_{2222} & D^{11}_{2222} & D^{01}_{2212} & D^{11}_{2212} & 0 & 0 & 0 & 0 & D^{1}_{2233} \\
D^{00}_{1211} & D^{01}_{1211} & D^{00}_{1222} & D^{01}_{1222} & D^{00}_{1212} & D^{01}_{1212} & 0 & 0 & 0 & 0 & D^{0}_{1233} \\
D^{01}_{1211} & D^{11}_{1211} & D^{01}_{1222} & D^{11}_{1222} & D^{01}_{1212} & D^{11}_{1212} & 0 & 0 & 0 & 0 & D^{1}_{1233} \\
0 & 0 & 0 & 0 & 0 & 0 & D^{00}_{1313} & D^{01}_{1313} & D^{00}_{1323} & D^{01}_{1323} & 0 \\
0 & 0 & 0 & 0 & 0 & 0 & D^{01}_{1313} & D^{11}_{1313} & D^{01}_{1323} & D^{11}_{1323} & 0 \\
0 & 0 & 0 & 0 & 0 & 0 & D^{00}_{2313} & D^{01}_{2313} & D^{00}_{2323} & D^{01}_{2323} & 0 \\
0 & 0 & 0 & 0 & 0 & 0 & D^{01}_{2313} & D^{11}_{2313} & D^{01}_{2323} & D^{11}_{2323} & 0 \\
D^{0}_{3311} & D^{1}_{3311} & D^{0}_{3322} & D^{1}_{3322} & D^{0}_{3312} & D^{1}_{3312} & 0 & 0 & 0 & 0 & D_{3333}
\end{bmatrix}, \tag{24}$$

$$\mathbf{v} = \begin{bmatrix} v^{-}_1 & v^{+}_1 & v^{-}_2 & v^{+}_2 & v^{-}_3 & v^{+}_3 \end{bmatrix}^{\mathrm{T}},$$

$$\mathbf{v}_{\Gamma} = \begin{bmatrix} v^{-}_v & v^{+}_v & v^{-}_t & v^{+}_t & v^{-}_3 & v^{+}_3 \end{bmatrix}^{\mathrm{T}},$$

$$\overset{\circ}{\boldsymbol{\mathscr{E}}} = \begin{bmatrix} \overset{\circ}{\mathscr{E}}{}^{-}_{11} & \overset{\circ}{\mathscr{E}}{}^{+}_{11} & \overset{\circ}{\mathscr{E}}{}^{-}_{22} & \overset{\circ}{\mathscr{E}}{}^{+}_{22} & 2\overset{\circ}{\mathscr{E}}{}^{-}_{12} & 2\overset{\circ}{\mathscr{E}}{}^{+}_{12} & 2\overset{\circ}{\mathscr{E}}{}^{-}_{13} & 2\overset{\circ}{\mathscr{E}}{}^{+}_{13} & 2\overset{\circ}{\mathscr{E}}{}^{-}_{23} & 2\overset{\circ}{\mathscr{E}}{}^{+}_{23} & \overset{\circ}{\mathscr{E}}{}_{33} \end{bmatrix}^{\mathrm{T}},$$

$$\mathbf{E} = \begin{bmatrix} E^{-}_{11} & E^{+}_{11} & E^{-}_{22} & E^{+}_{22} & 2E^{-}_{12} & 2E^{+}_{12} & 2E^{-}_{13} & 2E^{+}_{13} & 2E^{-}_{23} & 2E^{+}_{23} & E_{33} \end{bmatrix}^{\mathrm{T}},$$

$$\mathbf{H} = \begin{bmatrix} H^{-}_{11} & H^{+}_{11} & H^{-}_{22} & H^{+}_{22} & H^{-}_{12} & H^{+}_{12} & H^{-}_{13} & H^{+}_{13} & H^{-}_{23} & H^{+}_{23} & H_{33} \end{bmatrix}^{\mathrm{T}},$$

$$\hat{\mathbf{H}}_{\Gamma} = \begin{bmatrix} \hat{H}^{-}_{vv} & \hat{H}^{+}_{vv} & \hat{H}^{-}_{vt} & \hat{H}^{+}_{vt} & \hat{H}^{-}_{v3} & \hat{H}^{+}_{v3} \end{bmatrix}^{\mathrm{T}},$$

$$\mathbf{P} = \begin{bmatrix} -p^{-}_1 & p^{+}_1 & -p^{-}_2 & p^{+}_2 & -p^{-}_3 & p^{+}_3 \end{bmatrix}^{\mathrm{T}},$$

where $\mathbf{D}$ is the constitutive stiffness matrix whose components are defined in the next section; $A^{\mathrm{M}}_{\alpha} = A_{\alpha}(1 + k_{\alpha}\delta^{\mathrm{M}})$ are the Lamé coefficients of the middle surface S^{M}; $v^{\pm}_v$, $v^{\pm}_t$ and $v^{\pm}_3$ are the components of displacement vectors of face surfaces in the coordinate system v, t and α^3 (Fig. 1); k_{N} is the normal curvature of the reference bounding curve Γ; $H^{\pm}_{\alpha\beta}$, $H^{\pm}_{\alpha 3}$ and H_{33} are the stress resultants; $\hat{H}^{\pm}_{vv}$, $\hat{H}^{\pm}_{vt}$ and $\hat{H}^{\pm}_{v3}$ are the external load resultants defined as

$$H^{\pm}_{\alpha i} = \sum_k \int_{\delta_{k-1}}^{\delta_k} \sigma^{(k)}_{\alpha i} N^{\pm}\,\mathrm{d}\alpha^3, \quad H_{33} = \sum_k \int_{\delta_{k-1}}^{\delta_k} \sigma^{(k)}_{33}\,\mathrm{d}\alpha^3, \tag{25a}$$

$$\hat{H}^{\pm}_{v\text{æ}} = \sum_k \int_{\delta_{k-1}}^{\delta_k} q^{(k)}_{\text{æ}} N^{\pm}\,\mathrm{d}\alpha^3 \quad (\text{æ} = v, t \text{ and } 3). \tag{25b}$$

Mixed variational equation (23) will be used in Section 6 for constructing geometrically exact assumed stress–strain four-node curved solid-shell elements.

5. Constitutive equations

5.1. Complete constitutive equations

Consider the kth anisotropic layer of the shell and suppose that in each point there is a single surface of elastic symmetry parallel to the reference surface. In such case the equations of the complete 3D Hooke's law will be

$$\varepsilon_{ij} = \sum_{\ell,m} A^{(k)}_{ij\ell m}\sigma^{(k)}_{\ell m}, \tag{26}$$

where $A^{(k)}_{ij\ell m}$ are the components of the material tensor of the kth layer. Solving Eq. (26) for stresses one obtains the constitutive equations

$$\sigma^{(k)}_{\alpha\beta} = \sum_{\gamma,\delta} C^{(k)}_{\alpha\beta\gamma\delta}\varepsilon_{\gamma\delta} + C^{(k)}_{\alpha\beta 33}\varepsilon_{33}, \tag{27a}$$

$$\sigma^{(k)}_{\alpha 3} = 2\sum_{\gamma} C^{(k)}_{\alpha 3\gamma 3}\varepsilon_{\gamma 3}, \quad \sigma^{(k)}_{33} = \sum_{\gamma,\delta} C^{(k)}_{33\gamma\delta}\varepsilon_{\gamma\delta} + C^{(k)}_{3333}\varepsilon_{33}, \tag{27b}$$

where the following notations are used [20]:

$$C^{(k)}_{\alpha\beta\gamma\delta} = Q^{(k)}_{\alpha\beta\gamma\delta} + \frac{1}{\Lambda_k}\mu^{(k)}_{\alpha\beta 33}\mu^{(k)}_{33\gamma\delta}, \quad C^{(k)}_{\alpha\beta 33} = -\frac{1}{\Lambda_k}\mu^{(k)}_{\alpha\beta 33},$$

$$C^{(k)}_{33\alpha\beta} = -\frac{1}{\Lambda_k}\mu^{(k)}_{33\alpha\beta}, \tag{28a}$$

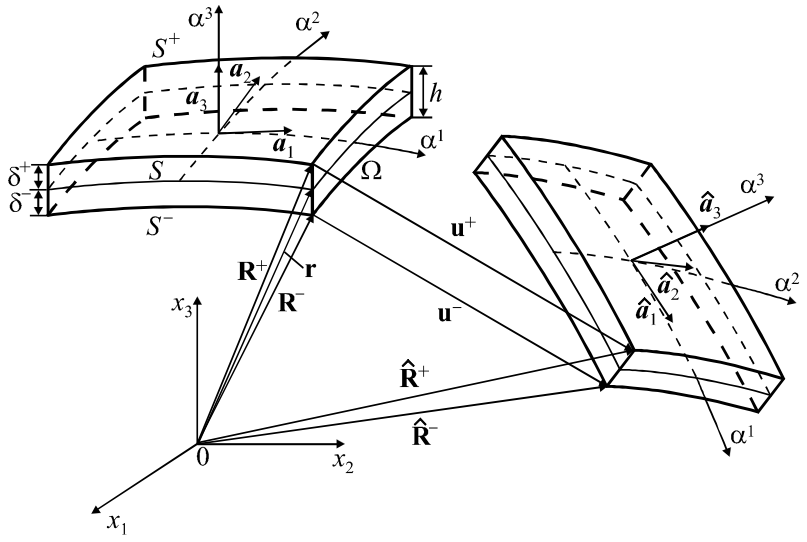

Fig. 2. Geometry and kinematics of shell.

$$C^{(k)}_{3333}=\frac{1}{\Lambda_k},\quad C^{(k)}_{1313}=\frac{1}{d_k}A^{(k)}_{2323},\quad C^{(k)}_{1323}=-\frac{1}{d_k}A^{(k)}_{1323},$$

$$C^{(k)}_{2323}=\frac{1}{d_k}A^{(k)}_{1313},$$

$$\mu^{(k)}_{\alpha\beta 33}=\sum_{\gamma,\delta}Q^{(k)}_{\alpha\beta\gamma\delta}A^{(k)}_{\gamma\delta 33},\quad \mu^{(k)}_{33\alpha\beta}=\sum_{\gamma,\delta}Q^{(k)}_{\gamma\delta\alpha\beta}A^{(k)}_{33\gamma\delta}, \tag{28b}$$

$$\Lambda_k=-\sum_{\gamma,\delta}A^{(k)}_{33\gamma\delta}\mu^{(k)}_{\gamma\delta 33}+A^{(k)}_{3333},\quad d_k=4\left(A^{(k)}_{1313}A^{(k)}_{2323}-A^{(k)}_{1323}A^{(k)}_{2313}\right),$$

$$Q^{(k)}_{1111}=\frac{1}{\Delta_k}\left(A^{(k)}_{2222}A^{(k)}_{1212}-A^{(k)}_{2212}A^{(k)}_{1222}\right),$$

$$Q^{(k)}_{1122}=\frac{1}{\Delta_k}\left(A^{(k)}_{1112}A^{(k)}_{1222}-A^{(k)}_{1122}A^{(k)}_{1212}\right), \tag{28c}$$

$$Q^{(k)}_{1112}=\frac{1}{2\Delta_k}\left(A^{(k)}_{1122}A^{(k)}_{2212}-A^{(k)}_{1112}A^{(k)}_{2222}\right),$$

$$Q^{(k)}_{2222}=\frac{1}{\Delta_k}\left(A^{(k)}_{1111}A^{(k)}_{1212}-A^{(k)}_{1112}A^{(k)}_{1211}\right),$$

$$Q^{(k)}_{2212}=\frac{1}{2\Delta_k}\left(A^{(k)}_{1112}A^{(k)}_{2211}-A^{(k)}_{1111}A^{(k)}_{2212}\right),$$

$$Q^{(k)}_{1212}=\frac{1}{4\Delta_k}\left(A^{(k)}_{1111}A^{(k)}_{2222}-A^{(k)}_{1122}A^{(k)}_{2211}\right),$$

$$\Delta_k=A^{(k)}_{1211}\left(A^{(k)}_{1122}A^{(k)}_{2212}-A^{(k)}_{1112}A^{(k)}_{2222}\right)+A^{(k)}_{1222}\left(A^{(k)}_{1112}A^{(k)}_{2211}-A^{(k)}_{1111}A^{(k)}_{2212}\right)$$
$$+A^{(k)}_{1212}\left(A^{(k)}_{1111}A^{(k)}_{2222}-A^{(k)}_{1122}A^{(k)}_{2211}\right).$$

Unfortunately, such six-parameter shell formulation on the basis of the complete 3D constitutive law (27) and (28) is deficient because thickness locking [10] can occur. This phenomenon occurs in bending dominated shell problems when Poisson's ratios are not equal to zero. The main reason is that Poisson's effect in the thickness direction is taken into account in equations of Hooke's law (26) for in-plane strains [15].

In order to prevent thickness locking at the finite element level an enhanced assumed strain concept [3,4,7] may be applied. There are alternative remedies in the literature based on the modification of 3D constitutive equations. Below these remedies are discussed concisely and assessed in Section 7 by means of a family of four-node curved shell elements developed.

5.2. Modified constitutive equations [9,19,20]

It is assumed that the transverse normal stress is constant in the thickness direction for every layer of the shell, i.e.,

$$\sigma^{(k)}_{33}=\frac{1}{h_k}H^{(k)}_{33},\quad H^{(k)}_{33}=\int_{\delta_{k-1}}^{\delta_k}\sigma^{(k)}_{33}\,\mathrm{d}\alpha^3, \tag{29}$$

where $H^{(k)}_{33}$ is the function depending on in-plane as well as thickness strains. Such assumption may be appreciated as a good remedy [9,19] for overcoming the thickness locking phenomenon. So, following this idea, one can derive from the 3D Hooke's law (26) and stress resultants (25a) the needed expressions for components of the modified constitutive stiffness matrix **D** [20]

$$D^{pq}_{\alpha\beta\gamma\delta}=\sum_k\left(n^{pq}_k Q^{(k)}_{\alpha\beta\gamma\delta}+\frac{n^p_k n^q_k \mu^{(k)}_{\alpha\beta 33}\mu^{(k)}_{33\gamma\delta}}{h_k\Lambda_k}\right),$$

$$D^{p}_{\alpha\beta 33}=-\sum_k\frac{1}{\Lambda_k}n^p_k\mu^{(k)}_{\alpha\beta 33},\quad D^{p}_{33\alpha\beta}=-\sum_k\frac{1}{\Lambda_k}n^p_k\mu^{(k)}_{33\alpha\beta},$$

$$D^{pq}_{\alpha 3\beta 3}=\sum_k n^{pq}_k C^{(k)}_{\alpha 3\beta 3},\quad D_{3333}=\sum_k\frac{1}{\Lambda_k}h_k,$$

$$n^{pq}_k=\int_{\delta_{k-1}}^{\delta_k}(N^-)^{2-p-q}(N^+)^{p+q}\,\mathrm{d}\alpha^3,$$

$$n^{p}_k=\int_{\delta_{k-1}}^{\delta_k}(N^-)^{1-p}(N^+)^{p}\,\mathrm{d}\alpha^3. \tag{30}$$

Throughout this section superscripts p, q take the values 0 and 1.

It should be mentioned that this modified constitutive law is quite efficient for most engineering problems. But for incompressible or nearly incompressible materials [10] some difficulties leading to volumetric locking can occur.

5.3. Reduced constitutive equations [13,15,20,22]

In order to circumvent simultaneously thickness and volumetric locking, we invoke a standard engineering assumption $\sigma_{33}^{(k)} \ll \sigma_{\alpha\beta}^{(k)}$ into equations of Hooke's law (26) for the in-plane strains. This implies that components of the material tensor $A_{\alpha\beta 33}^{(k)} = 0$. At the same time the last equation for the thickness strain (26) is left unchanged, i.e., $A_{33\alpha\beta}^{(k)} \neq 0$. Allowing for this simplification, the following expressions for components of the reduced constitutive stiffness matrix **D** are obtained [20]:

$$D_{\alpha\beta\gamma\delta}^{pq} = \sum_k n_k^{pq} Q_{\alpha\beta\gamma\delta}^{(k)}, \quad D_{\alpha\beta 33}^{p} = 0, \quad D_{33\alpha\beta}^{p} = -\sum_k \frac{1}{A_{3333}^{(k)}} n_k^{p} \mu_{33\alpha\beta}^{(k)},$$
$$D_{\alpha 3\beta 3}^{pq} = \sum_k n_k^{pq} C_{\alpha 3\beta 3}^{(k)}, \quad D_{3333} = \sum_k \frac{1}{A_{3333}^{(k)}} h_k. \tag{31}$$

Note that relations (31) follow from (30), since $\mu_{\alpha\beta 33}^{(k)} = 0$ and $\Lambda_k = A_{3333}^{(k)}$ according to Eq. (28b).

The reduced constitutive law was proposed by Kulikov [22] and showed a good performance in case of using six-parameter plate and shell models [13,15]. It should be observed that this approach yields the non-symmetric material matrix and as a result more computational efforts have to be made.

5.4. Simplified constitutive equations [1,2,14,20]

When a shell is undergone pure bending, one half of the shell body in the thickness direction is under tension and the other half is under compression, i.e., the thickness strain according to the 3D Hooke's law would be zero due to limitation of the linear displacement approximation (4). So, a shell will be in the plane strain state instead of the expected plane stress state. In order to circumvent these difficulties, the simplified constitutive stiffness matrix **D** can be employed [20]

$$D_{\alpha\beta\gamma\delta}^{pq} = \sum_k n_k^{pq} Q_{\alpha\beta\gamma\delta}^{(k)}, \quad D_{\alpha\beta 33}^{p} = D_{33\alpha\beta}^{p} = 0,$$
$$D_{\alpha 3\beta 3}^{pq} = \sum_k n_k^{pq} C_{\alpha 3\beta 3}^{(k)}, \quad D_{3333} = \sum_k \frac{1}{A_{3333}^{(k)}} h_k. \tag{32}$$

This is due to the plane stress enforcement which is done by decoupling the transverse normal stress with all other stresses in the 3D Hooke's law (26) [1,2], i.e., it is supposed that $A_{\alpha\beta 33}^{(k)} = A_{33\alpha\beta}^{(k)} = 0$.

It is apparent that the simplified constitutive law leads to the symmetric constitutive stiffness matrix **D** but it is slightly deficient for the thick anisotropic shells. So, allowing for simplicity of such approach it may be recommended for analysis of composite thin-walled structures.

Further all three remedies for overcoming thickness locking (30)–(32) are evaluated with several discriminating problems selected from the literature.

6. Finite element formulation

Here, we address concisely the computational aspects of the six-parameter anisotropic ESL shell theory. For this purpose we write the mixed variational Eq. (23) for the shell element as follows:

$$\int_{-1}^{1}\int_{-1}^{1} [\delta\mathbf{E}^{\mathrm{T}}(\mathbf{H} - \mathbf{D}\mathbf{E}) + \delta\mathbf{H}^{\mathrm{T}}(\mathbf{E} - \boldsymbol{\mathscr{E}}) - \delta\boldsymbol{\mathscr{E}}^{\mathrm{T}}\mathbf{H} + \delta\mathbf{v}^{\mathrm{T}}\mathbf{P}] A_1^{\mathrm{M}e\ell} A_2^{\mathrm{M}e\ell}\, \mathrm{d}\xi_1\, \mathrm{d}\xi_2 + \oint_{\Gamma^{e\ell}} \delta\mathbf{v}_\Gamma^{\mathrm{T}} \hat{\mathbf{H}}_\Gamma (1 + k_{\mathrm{N}}\delta^{\mathrm{M}})\, \mathrm{d}s = 0, \tag{33}$$

where $A_\gamma^{\mathrm{M}e\ell} = A_\gamma^{\mathrm{M}} \ell_\gamma^{e\ell}$ are the Lamé coefficients of the middle surface $S^{\mathrm{M}e\ell}$ of the element; $\xi_\gamma = (\alpha_\gamma - d_\gamma^{e\ell})/\ell_\gamma^{e\ell}$ are the local curvilinear normalized coordinates (Fig. 3); $d_\gamma^{e\ell} = (\alpha_\gamma^{-e\ell} + \alpha_\gamma^{+e\ell})/2$ are the coordinates of the center of the element; $2\ell_\gamma^{e\ell} = \alpha_\gamma^{+e\ell} - \alpha_\gamma^{-e\ell}$ are the lengths of the element and $\alpha_\gamma = \alpha^\gamma$.

For the simplest four-node shell element the displacement field is approximated according to the standard C^0 interpolation

$$\mathbf{v} = \sum_r N_r \mathbf{v}_r \quad \text{or} \quad \mathbf{v} = \sum_{r_1 r_2} \xi_1^{r_1} \xi_2^{r_2} \mathbf{v}^{r_1 r_2}, \tag{34}$$

where $\mathbf{v}_r = \begin{bmatrix} v_{1r}^- & v_{1r}^+ & v_{2r}^- & v_{2r}^+ & v_{3r}^- & v_{3r}^+ \end{bmatrix}^{\mathrm{T}}$ are the displacement vectors of the element nodes; $N_r(\xi_1, \xi_2)$ are the bilinear shape functions of the element; the index r runs from 1 to 4 and denotes a number of nodes. Throughout this section superscripts r_1, r_2 take the values 0 and 1.

In a result for the displacement-dependent strains (20) we have the following approximation [25]:

$$\boldsymbol{\mathscr{E}} = \sum_{r_1 r_2} \xi_1^{r_1} \xi_2^{r_2} \boldsymbol{\mathscr{E}}^{r_1 r_2}, \quad \boldsymbol{\mathscr{E}}^{r_1 r_2} = \mathbf{B}^{r_1 r_2} \mathbf{V},$$
$$\boldsymbol{\mathscr{E}}^{r_1 r_2} = \begin{bmatrix} \overset{\circ}{\mathscr{E}}{}_{11}^{-r_1 r_2} & \overset{\circ}{\mathscr{E}}{}_{11}^{+r_1 r_2} & \overset{\circ}{\mathscr{E}}{}_{22}^{-r_1 r_2} & \overset{\circ}{\mathscr{E}}{}_{22}^{+r_1 r_2} & 2\overset{\circ}{\mathscr{E}}{}_{12}^{-r_1 r_2} & 2\overset{\circ}{\mathscr{E}}{}_{12}^{+r_1 r_2} \\ 2\overset{\circ}{\mathscr{E}}{}_{13}^{-r_1 r_2} & 2\overset{\circ}{\mathscr{E}}{}_{13}^{+r_1 r_2} & 2\overset{\circ}{\mathscr{E}}{}_{23}^{-r_1 r_2} & 2\overset{\circ}{\mathscr{E}}{}_{23}^{+r_1 r_2} & \overset{\circ}{\mathscr{E}}{}_{33}^{r_1 r_2} \end{bmatrix}^{\mathrm{T}}, \tag{35}$$

where $\mathbf{V} = \begin{bmatrix} \mathbf{v}_1^{\mathrm{T}} & \mathbf{v}_2^{\mathrm{T}} & \mathbf{v}_3^{\mathrm{T}} & \mathbf{v}_4^{\mathrm{T}} \end{bmatrix}^{\mathrm{T}}$ is the displacement vector at nodal points of the element; $\mathbf{B}^{r_1 r_2}$ are the matrices of order 11×24 corresponding to the strain–displacement transformation.

To avoid shear and membrane locking and have no spurious zero energy modes, the assumed strain and stress resultant fields [15] inside the element are introduced

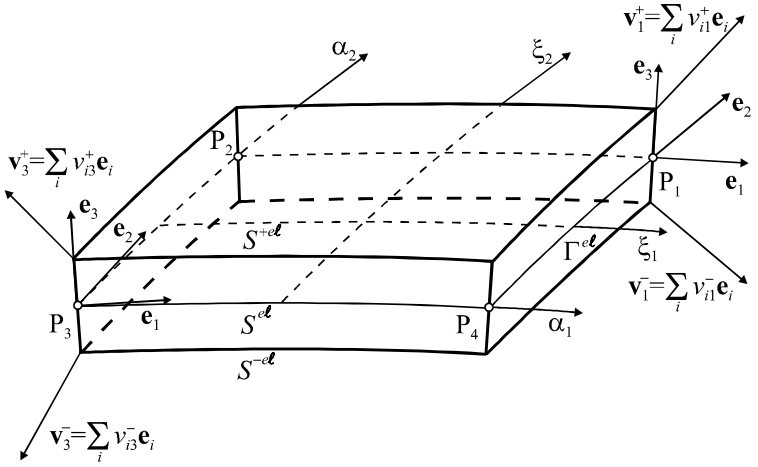

Fig. 3. Four-node geometrically exact solid-shell element.

$$\mathbf{E}=\sum_{r_1,r_2}\xi_1^{r_1}\xi_2^{r_2}\mathbf{Q}^{r_1r_2}\mathbf{E}^{r_1r_2}, \tag{36a}$$

$$\mathbf{E}^{00}=\begin{bmatrix}E_{11}^{-00} & E_{11}^{+00} & E_{22}^{-00} & E_{22}^{+00} & 2E_{12}^{-00} & 2E_{12}^{+00}\\ 2E_{13}^{-00} & 2E_{13}^{+00} & 2E_{23}^{-00} & 2E_{23}^{+00} & E_{33}^{00}\end{bmatrix}^{\mathrm{T}},$$

$$\mathbf{E}^{01}=\begin{bmatrix}E_{11}^{-01} & E_{11}^{+01} & 2E_{13}^{-01} & 2E_{13}^{+01} & E_{33}^{01}\end{bmatrix}^{\mathrm{T}},$$

$$\mathbf{E}^{10}=\begin{bmatrix}E_{22}^{-10} & E_{22}^{+10} & 2E_{23}^{-10} & 2E_{23}^{+10} & E_{33}^{10}\end{bmatrix}^{\mathrm{T}},\quad \mathbf{E}^{11}=\begin{bmatrix}E_{33}^{11}\end{bmatrix},$$

$$\mathbf{H}=\sum_{r_1,r_2}\xi_1^{r_1}\xi_2^{r_2}\mathbf{Q}^{r_1r_2}\mathbf{H}^{r_1r_2}, \tag{36b}$$

$$\mathbf{H}^{00}=\begin{bmatrix}H_{11}^{-00} & H_{11}^{+00} & H_{22}^{-00} & H_{22}^{+00} & H_{12}^{-00} & H_{12}^{+00}\\ H_{13}^{-00} & H_{13}^{+00} & H_{23}^{-00} & H_{23}^{+00} & H_{33}^{00}\end{bmatrix}^{\mathrm{T}},$$

$$\mathbf{H}^{01}=\begin{bmatrix}H_{11}^{-01} & H_{11}^{+01} & H_{13}^{-01} & H_{13}^{+01} & H_{33}^{01}\end{bmatrix}^{\mathrm{T}},$$

$$\mathbf{H}^{10}=\begin{bmatrix}H_{22}^{-10} & H_{22}^{+10} & H_{23}^{-10} & H_{23}^{+10} & H_{33}^{10}\end{bmatrix}^{\mathrm{T}},\quad \mathbf{H}^{11}=\begin{bmatrix}H_{33}^{11}\end{bmatrix},$$

where $\mathbf{Q}^{00}$ is the identity matrix of order 11×11, while $\mathbf{Q}^{01}$, $\mathbf{Q}^{10}$ and $\mathbf{Q}^{11}$ are the matrices of order 11×5 and 11×1, respectively, defined in papers [15,25].

Substituting approximations (34)–(36) into the mixed variational Eq. (33) and eliminating strains $\mathbf{E}^{r_1r_2}$ and stress resultants $\mathbf{H}^{r_1r_2}$, one arrives at the element equilibrium equations

$$\mathbf{KV}=\mathbf{F}, \tag{37}$$

where $\mathbf{F}$ is the force vector and $\mathbf{K}$ is the elemental stiffness matrix defined as

$$\mathbf{K}=\sum_{r_1,r_2}\frac{1}{3^{r_1+r_2}}(\mathbf{B}^{r_1r_2})^{\mathrm{T}}\mathbf{Q}^{r_1r_2}(\mathbf{Q}^{r_1r_2})^{\mathrm{T}}\mathbf{D}\mathbf{Q}^{r_1r_2}(\mathbf{Q}^{r_1r_2})^{\mathrm{T}}\mathbf{B}^{r_1r_2}. \tag{38}$$

All three elemental stiffness matrices developed (see Section 5) have six, and only six, zero eigenvalues as required for satisfaction of the general rigid-body motion representation. It should be mentioned that our stiffness matrices (38) require only direct substitutions, i.e., no inversion is needed if sides of the element coincide with lines of principal curvatures of the reference surface. Furthermore, they are evaluated by using the 3D analytical integration. So, our finite element formulation is very economical and efficient compared to the conventional isoparametric finite element formulations because it reduces the costly numerical integration by deriving the elemental stiffness matrices [26–28].

In order to fulfill an analytical integration, we invoke non-traditional schemes [25] for computation of the face surface strains (35) accounting for relations (20) and (21)

$$\begin{aligned}2\overset{\circ}{\mathscr{E}}{}_{\alpha\beta}^{\pm r_1r_2}&=\left\{\zeta_\alpha^{\pm}\right\}^{00}\lambda_{\alpha\beta}^{\pm r_1r_2}+\left\{\zeta_\beta^{\pm}\right\}^{00}\lambda_{\beta\alpha}^{\pm r_1r_2},\\ 2\overset{\circ}{\mathscr{E}}{}_{\alpha3}^{\pm r_1r_2}&=\left\{\zeta_\alpha^{\pm}\right\}^{00}\beta_\alpha^{r_1r_2}-\theta_\alpha^{\pm r_1r_2},\quad \overset{\circ}{\mathscr{E}}{}_{33}^{r_1r_2}=\beta_3^{r_1r_2},\end{aligned} \tag{39}$$

where

$$\begin{aligned}\lambda_{\alpha\alpha}^{\pm r_1r_2}&=\left\{\frac{1}{A_\alpha^{e\ell}}v_\alpha^{\pm}\right\}_\alpha^{r_1r_2}+\left\{B_{\alpha\alpha}^{e\ell}v_\alpha^{\pm}+B_{\alpha\beta}^{e\ell}v_\beta^{\pm}+k_\alpha v_3^{\pm}\right\}^{r_1r_2}\quad(\beta\neq\alpha),\\ \lambda_{\beta\alpha}^{\pm r_1r_2}&=\left\{\frac{1}{A_\alpha^{e\ell}}v_\beta^{\pm}\right\}_\alpha^{r_1r_2}+\left\{B_{\alpha\alpha}^{e\ell}v_\beta^{\pm}-B_{\alpha\beta}^{e\ell}v_\alpha^{\pm}\right\}^{r_1r_2}\quad(\beta\neq\alpha),\\ \theta_\alpha^{\pm r_1r_2}&=-\left\{\frac{1}{A_\alpha^{e\ell}}v_3^{\pm}\right\}_\alpha^{r_1r_2}+\left\{-B_{\alpha\alpha}^{e\ell}v_3^{\pm}+k_\alpha v_\alpha^{\pm}\right\}^{r_1r_2},\quad \beta_i^{r_1r_2}=\frac{1}{h}\left\{v_i^+-v_i^-\right\}^{r_1r_2}.\end{aligned} \tag{40}$$

In formulas (39) and (40) in accordance with Fig. 3 convenient mesh notations are used

$$\{f\}^{00}=\frac{1}{4}[f(P_1)+f(P_2)+f(P_3)+f(P_4)],$$

$$\{f\}^{01}=\frac{1}{4}[f(P_1)+f(P_2)-f(P_3)-f(P_4)],$$

$$\{f\}^{10}=\frac{1}{4}[f(P_1)-f(P_2)-f(P_3)+f(P_4)],$$

$$\{f\}^{11} = \frac{1}{4}[f(P_1) - f(P_2) + f(P_3) - f(P_4)],$$
$$\{f\}_1^{00} = \{f\}^{10}, \quad \{f\}_1^{01} = \{f\}^{11}, \quad \{f\}_1^{10} = \{f\}_1^{11} = 0,$$
$$\{f\}_2^{00} = \{f\}^{01}, \quad \{f\}_2^{10} = \{f\}^{11}, \quad \{f\}_2^{01} = \{f\}_2^{11} = 0. \tag{41}$$

As regards a product $A_1^{Me\ell}A_2^{Me\ell}$ from the variational Eq. (33), it does not vary inside the element and with account for notations (41) the simplest approximation is employed

$$A_1^{Me\ell}A_2^{Me\ell} = \{A_1^{Me\ell}A_2^{Me\ell}\}^{00}. \tag{42}$$

7. Numerical tests

The performance of the proposed four-node geometrically exact solid-shell elements is evaluated with several problems extracted from the literature. A listing of these elements and the abbreviations used to identify them are contained in Table 1. The computational merits of the developed analytical integration schemes are demonstrated by comparing CPU time required by the TMS4SA and TMS4SN elements in case of the homogeneous shell and laminated composite one as well. Here, for conciseness, only one four-node solid-shell element, based on the Gauss numerical integration scheme, namely, TMS4SN is presented. The remaining elements on the basis of the numerical integration exhibit close predictions and are not discussed in the present paper. It should be mentioned that the approximation (42) has been employed and for this type of the geometrically exact solid-shell elements.

Table 1
Listing of developed four-node geometrically exact solid-shell elements (see Section 5)

Name	Description
TMS4MA	Four-node element based on the modified constitutive law (30) and analytical integration
TMS4RA	Four-node element based on the reduced constitutive law (31) and analytical integration
TMS4SA	Four-node element based on the simplified constitutive law (32) and analytical integration
TMS4SN	Four-node element based on the simplified constitutive law (32) and 2×2 Gauss numerical integration scheme

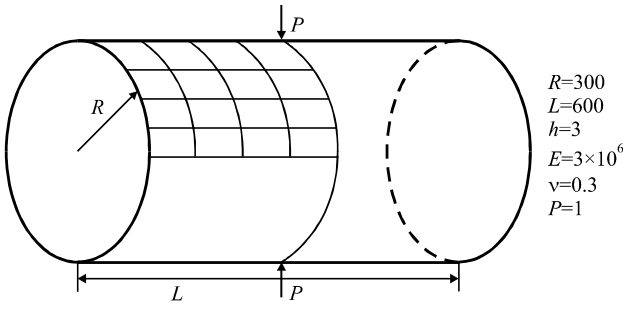

Shell of revolution with geometrical parameters:
$A_1=1,\ A_2=R,\ k_1=0,\ k_2=1/R,\ \alpha_1\in[0, L/2],\ \alpha_2\in[0, \pi/2]$

Fig. 4. Pinched cylindrical shell.

7.1. Pinched cylindrical shell with rigid diaphragms

To illustrate the capability of developed four-node elements to overcome membrane and shear locking phenomena and to compare them with high performance four-node quadrilateral elements [29–32], we consider one of the most demanding standard linear tests. A short cylindrical shell supported by two rigid diaphragms at the ends is loaded by two opposite concentrated forces in its middle section. The geometrical and material properties of the shell are shown in Fig. 4.

Owing to symmetry of the problem, only one octant of the shell is modeled with regular meshes of proposed elements. Table 2 displays the normalized transverse displacement under the applied load and a comparison with above four-node quadrilateral elements. The displacements are normalized with respect to the analytical solution -1.8248×10^{-5} [33]. As can be seen, our results exhibit an excellent agreement even for coarse meshes. Additionally, Table 3 lists the computational performance of the proposed analytical integration schemes (39)–(41). As it turned out, CPU time required for the formation of the

Table 3
CPU time (in dimensionless units) required for evaluation of global stiffness matrix by TMS4 elements with analytical and numerical integration schemes

Mesh	Cylindrical shell		Hyperbolic shell	
	TMS4SA	TMS4SN	TMS4SA	TMS4SN
4×4	1	1.50	1	1.50
16×16	1	1.51	1	1.50

Table 2
Normalized transverse displacement $(v_3^M)^{Norm}$ under applied load of pinched cylindrical shell

Mesh	Isoparametric four-node elements				TMS4 elements			
	[29]	[30]	[31]	[32]	TMS4MA	TMS4RA	TMS4SA	TMS4SN
4×4	0.373	0.469	0.370	0.399	0.8881	0.8902	0.8900	0.8900
8×8	0.747	0.791	0.740	0.763	0.9406	0.9414	0.9412	0.9412
16×16	0.935	0.946	0.930	0.935	0.9862	0.9863	0.9861	0.9861

global stiffness matrix is slightly dependent on a number of elements used for discretizing a shell and the TMS4SN element needs about 50% more time than the TMS4SA one.

7.2. Angle-ply cylindrical shell subjected to uniform stretching

To evaluate the transverse normal deformation and anisotropy shell response, we consider relatively thick two- and three-layer angle-ply cylindrical shells subjected to uniform end stretching [23], as shown in Fig. 5. The shell is assumed to be rigidly clamped at $\alpha_1 = -50$ and $\alpha_1 = 50$. The material characteristics of the individual ply are presented in Fig. 5, where subscripts L and T refer to the fiber and transverse directions. The ply angle γ between the fiber direction and α_1-axis is measured in the clockwise direction.

Due to the anisotropic shell response, we did not adopt symmetry conditions, as in the previous example, and modeled the whole cylindrical shell by using regular meshes of the axisymmetric TMS4 elements. Table 4 lists the normalized transverse displacement of the middle surface and thickness change $\Delta h = v_3^+ - v_3^-$ at the central section of the shell (at $\alpha_1 = 0$) for the ply angle $\gamma = 30°$. The displacement and thickness change have been normalized with respect to the exact values of $v_3^{\mathrm{M}}/u_0 = -4.3700$ and $\Delta h/u_0 = 0.0210$ [23], which were derived by using a close ESL

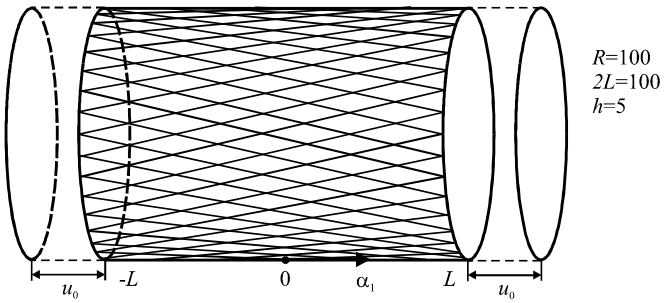

Fig. 5. Angle-ply cylindrical shell subjected to uniform stretching.

Table 4
Normalized transverse displacement and thickness change at central section of two-layer angle-ply cylindrical shell subjected to uniform stretching for ply angle $\gamma = 30°$

Mesh	$(v_3^{\mathrm{M}})^{\mathrm{Norm}}$			$(\Delta h)^{\mathrm{Norm}}$		
	TMS4MA	TMS4RA	TMS4SA	TMS4MA	TMS4RA	TMS4SA
4×1	1.0086	1.0102	1.0100	1.2583	1.2666	0.08464
8×1	1.0016	1.0027	1.0025	1.0218	1.0267	0.04932
16×1	0.9976	0.9988	0.9985	0.9982	1.0025	0.04557
32×1	0.9965	0.9977	0.9974	0.9943	0.9986	0.04492

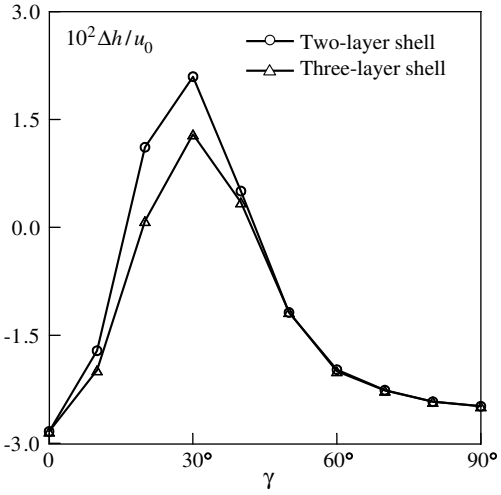

Fig. 6. Thickness change $\Delta h = v_3^+ - v_3^-$ at central section of cylindrical shell versus ply angle γ.

theory based on the strain–displacement relations (20) with $\zeta_\alpha^{\pm} = 1$. It is apparent that such relations cannot represent rigid-body motions precisely. Note that the simplified constitutive law (32) leads to the poor prediction of the composite shell response. Additionally, Fig. 6 displays the thickness change Δh at the central section versus an angle γ by using the 32×1 mesh of TMS4RA elements. As can be seen, the shell behaviour is very unusual to the region $20° < \gamma < 40°$ especially for the two-layer shell, where Δh is *positive* and has a maximum value.

7.3. Pinched cross-ply hyperbolic shell

A three-layer cross-ply hyperbolic shell under two pairs of opposite concentrated forces was considered by Basar et al. [34] for testing finite deformation formulations for composite shells, while we employ this example as a linear benchmark test to assess the proposed schemes of the analytical integration. Besides, as in the pinched cylinder example we can verify a proper representation of inextensional bending and, additionally, this is an excellent test for the ability of the element to model rigid-body motions. The geometrical and material data of the three-layer hyperbolic shell are given in Fig. 7, where the fiber (L) direction coincides with the circumferential one in outer layers.

Owing to symmetry, only one octant of the shell is discretized with uniform meshes of developed elements. Table 5 lists normalized displacements at points A and C. The displacements are normalized with respect to values $-v_y^{\mathrm{MA}} = v_x^{\mathrm{MB}} = 0.1013$ and $v_y^{\mathrm{MC}} = -v_x^{\mathrm{MD}} = 0.09785$, respectively, where v_x^{M} and v_y^{M} denote displacements of the middle surface in x and y directions. Such values are the answers based on the proposed geometrically exact shell model with account for the simplified constitutive law, i.e., the TMS4SA element and consistent mesh refinements have been used. One can observe that developed schemes of

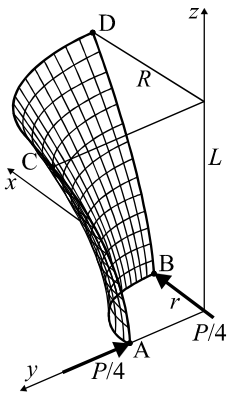

$r = 7.5$
$R = 15$
$L = 20$
$h = 0.04$
$h_0 = h/3$
$E_L = 4\times10^7$
$E_T = 10^6$
$G_{LT} = G_{TT} = 6\times10^5$
$\nu_{LT} = \nu_{TT} = 0.25$
$P = 4$
Ply thickness $= [h_0/h_0/h_0]$
Ply orientation $= [90/0/90]$

Shell of revolution with geometrical parameters:

$$A_1 = \sqrt{1+\frac{\mu^2 z^2}{A_2^2}},\quad A_2 = r\sqrt{1+\frac{\mu z^2}{r^2}},\quad k_1 = -\frac{\mu r^2}{A_1^3 A_2^3},$$

$$k_2 = \frac{1}{A_1 A_2},\quad \mu = \frac{R^2 - r^2}{L^2},\quad \alpha_1 = z \in [0, L],\quad \alpha_2 \in [0, \pi/2]$$

Fig. 7. Pinched three-layer cross-ply hyperbolic shell.

the analytical integration perform very well. See also data in Table 3 concerning CPU time required for the formation of the stiffness matrix.

7.4. Angle-ply hyperbolic shell subjected to uniform stretching

It is known that for a hyperbolic surface there are exactly two asymptotic directions, which lie in between the directions of principal curvatures, i.e., two families of *straight lines* are contained in a surface. These lines provide the asymptotic directions at all of surface points. If fiber directions would coincide with the asymptotic line directions then one could build a thin-walled structure that would be suitable for many engineering applications. Let the ply angle γ between the asymptotic line and the tangent to the meridian be measured in the clockwise direction. This angle may be evaluated by means of a simple formula displayed in Fig. 8 in accordance with notations in Fig. 7.

So, we consider such kind of two- and three-layer angle-ply hyperbolic shells subjected to uniform stretching as shown in Fig. 8. It is assumed that shell ends are rigidly

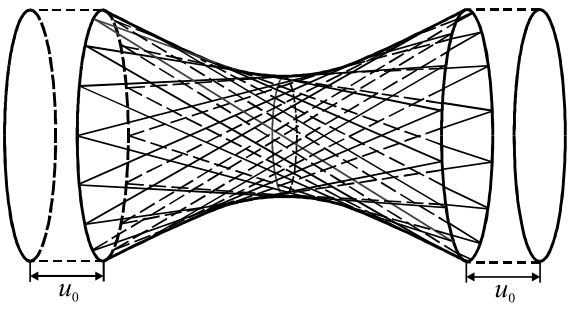

Ply thickness=[0.02/0.02] and [0.01/0.02/0.01]
Ply orientation=[γ/-γ] and [γ/-γ/γ], $\cos\gamma = A_1/\sqrt{1+\mu}$

Fig. 8. Angle-ply hyperbolic shell subjected to uniform stretching.

Table 6
Normalized displacements at sections $\alpha_1 = \pm L/2$ of two-layer angle-ply hyperbolic shell subjected to uniform stretching

Mesh	TMS4MA		TMS4RA		TMS4SA	
	$(v_2^M)^{Norm}$	$(v_3^M)^{Norm}$	$(v_2^M)^{Norm}$	$(v_3^M)^{Norm}$	$(v_2^M)^{Norm}$	$(v_3^M)^{Norm}$
4×1	2.4456	0.5072	2.4434	0.5085	2.4456	0.5086
8×1	1.2895	1.3068	1.2906	1.3070	1.2920	1.3070
16×1	1.1145	1.0692	1.1181	1.0694	1.1192	1.0694
32×1	1.0149	1.0154	1.0145	1.0154	1.0153	1.0154

clamped. This problem has been chosen for numerical testing the anisotropic shell element behaviour. The geometrical characteristics of the shell and material properties of the individual ply are given in Fig. 7 but ply thicknesses are taken to be different, in order to compose the self-equilibrated structure.

Here, we did not adopt symmetry conditions and modeled the whole hyperbolic shell by using regular meshes of the axisymmetric TMS4 elements. Table 6 lists results of the convergence study, where circumferential and transverse displacements at sections $\alpha_1 = \pm L/2$ are normalized with respect to the computationally exact values $v_2^M/u_0 = -0.8962\times10^{-3}$ and $v_3^M/u_0 = -0.1968$ (see for this subject Section 7.3). It should be noted that these results cannot be easily achieved by the conventional isoparametric elements with such coarse mesh configuration. Figs. 9 and 10 show displacements and transverse shear strains of the middle surface versus a coordinate α_1 employing the 32×1 mesh of TMS4SA elements.

Table 5
Normalized displacements at points A and C of pinched three-layer cross-ply hyperbolic shell

Mesh	TMS4MA		TMS4RA		TMS4SA		TMS4SN	
	$(v_y^{MA})^{Norm}$	$(v_y^{MC})^{Norm}$	$(v_y^{MA})^{Norm}$	$(v_y^{MC})^{Norm}$	$(v_y^{MA})^{Norm}$	$(v_y^{MC})^{Norm}$	$(v_y^{MA})^{Norm}$	$(v_y^{MC})^{Norm}$
2×2	0.5941	1.1436	0.5961	1.1474	0.5961	1.1474	0.3720	0.5448
4×4	0.8694	1.0299	0.8726	1.0337	0.8726	1.0337	0.8331	0.9324
8×8	0.9575	1.0052	0.9610	1.0089	0.9610	1.0089	0.9700	1.0031
16×16	0.9842	0.9983	0.9881	1.0020	0.9879	1.0021	0.9906	1.0010

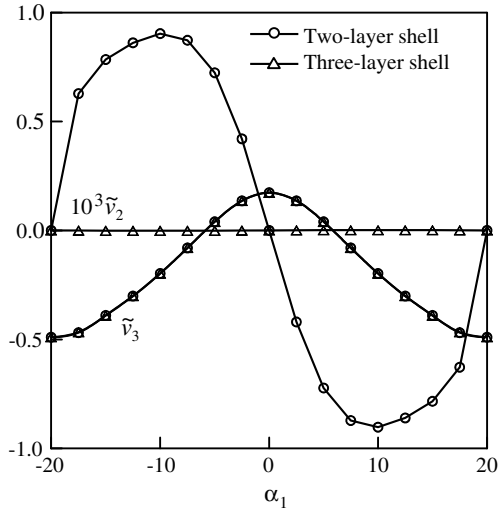

Fig. 9. Circumferential and transverse displacements of middle surface $\tilde{v}_{\alpha+1} = v^{M}_{\alpha+1}/u_0$ of hyperbolic shell versus coordinate α_1.

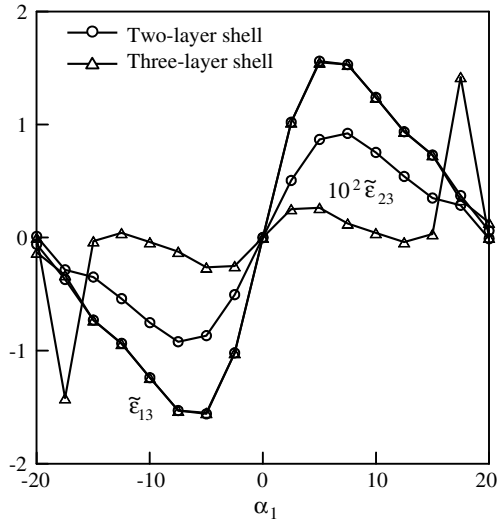

Fig. 10. Transverse shear strains of middle surface $\tilde{\varepsilon}_{\alpha 3} = 50L\varepsilon^{M}_{\alpha 3}/u_0$ of hyperbolic shell versus coordinate α_1.

8. Conclusions

The new geometrically exact multilayered solid-shell models have been developed. These models are based on the objective strain–displacement relationships represented in the general curvilinear coordinates and, therefore, may be used for the formulation of effective curved multilayered solid-shell elements. However, the practical use of such elements requires the development of constitutive equations, in order to overcome the thickness locking phenomenon.

The simple and efficient assumed stress–strain four-node curved shell elements are based on the original approach, in which displacement vectors of the face surfaces are introduced and resolved, as in classical shell formulations, in the reference surface frame. All three elements developed do not contain any spurious zero energy modes and possess six zero eigenvalues. It is remarkable that all constructed elemental stiffness matrices require only direct substitutions (no inversion is needed) and they are evaluated by using the 3D analytical integration. Therefore, our formulation is very simple and economical compared to conventional isoparametric formulations.

Acknowledgement

The present research was supported by Russian Fund of Basic Research (Grant No. 04-01-00070).

References

[1] Ausserer MF, Lee SW. An eighteen-node solid element for thin shell analysis. Int J Numer Meth Eng 1988;26:1345–64.
[2] Kim YH, Lee SW. A solid element formulation for large deflection analysis of composite shell structures. Comput Struct 1988;30:269–74.
[3] Buchter N, Ramm E, Roehl D. Three-dimensional extension of nonlinear shell formulation based on the enhanced assumed strain concept. Int J Numer Meth Eng 1994;37:2551–68.
[4] Braun M, Bischoff M, Ramm E. Nonlinear shell formulations for complete three-dimensional constitutive laws including composites and laminates. Comput Mech 1994;15:1–18.
[5] Parisch H. A continuum-based shell theory for non-linear applications. Int J Numer Meth Eng 1995;38:1855–83.
[6] Park HC, Cho C, Lee SW. An efficient assumed strain element model with six dof per node for geometrically nonlinear shells. Int J Numer Meth Eng 1995;38:4101–22.
[7] Betsch P, Stein E. An assumed strain approach avoiding artificial thickness straining for a nonlinear 4-node shell element. Commun Numer Meth Eng 1995;11:899–909.
[8] Hauptmann R, Schweizerhof K. A systematic development of 'solid-shell' element formulations for linear and non-linear analyses employing only displacement degrees of freedom. Int J Numer Meth Eng 1998;42:49–69.
[9] Sze KY, Chan WK, Pian THH. An eight-node hybrid-stress solid-shell element for geometric non-linear analysis of elastic shells. Int J Numer Meth Eng 2002;55:853–78.
[10] Sze KY. Three-dimensional continuum finite element models for plate/shell analysis. Prog Struct Eng Mater 2002;4:400–7.
[11] Kulikov GM, Plotnikova SV. Finite element formulation of straight composite beams undergoing finite rotations. Trans Tambov State Tech Univ 2001;7:617–33.
[12] Kulikov GM, Plotnikova SV. Non-conventional non-linear two-node hybrid stress–strain curved beam elements. Finite Elements Anal Des 2004;40:1333–59.
[13] Kulikov GM, Plotnikova SV. Finite deformation plate theory and large rigid-body motions. Int J Non-Linear Mech 2004;39:1093–109.
[14] Kulikov GM, Plotnikova SV. Simple and effective elements based upon Timoshenko–Mindlin shell theory. Comput Meth Appl Mech Eng 2002;191:1173–87.
[15] Kulikov GM, Plotnikova SV. Non-linear strain–displacement equations exactly representing large rigid-body motions. Part I. Timoshenko–Mindlin shell theory. Comput Meth Appl Mech Eng 2003; 192:851–75.
[16] Roh HY, Cho M. The application of geometrically exact shell elements to B-spline surfaces. Comput Meth Appl Mech Eng 2004;193:2261–99.
[17] Simo JC, Rifai MS, Fox DD. On a stress resultant geometrically exact shell model. Part IV. Variable thickness shells with through-the-thickness stretching. Comput Meth Appl Mech Eng 1990;81:91–126.
[18] Wempner G, Talaslidis D, Hwang CM. A simple and efficient approximation of shells via finite quadrilateral elements. J Appl Mech 1982;49:115–20.

[19] Pian THH. Finite elements based on consistently assumed stresses and displacements. Finite Elements Anal Des 1985;1: 131–40.
[20] Kulikov GM, Plotnikova SV. Equivalent single-layer and layer-wise shell theories and rigid-body motions—Part I: Foundations. Mech Advanced Mater Struct 2005;12:275–83.
[21] Sze KY, Yi S, Tay MH. An explicit hybrid stabilized eighteen-node solid element for thin shell analysis. Int J Numer Meth Eng 1997; 40:1839–56.
[22] Kulikov GM. Analysis of initially stressed multilayered shells. Int J Solids Struct 2001;38:4535–55.
[23] Kulikov GM. Refined global approximation theory of multilayered plates and shells. J Eng Mech 2001;127:119–25.
[24] Washizu K. Variational methods in elasticity and plasticity. 3rd ed. Oxford: Pergamon Press; 1982.
[25] Kulikov GM, Plotnikova SV. Equivalent single-layer and layer-wise shell theories and rigid-body motions—Part II: Computational aspects. Mech Advanced Mater Struct 2005;12:331–40.
[26] Hughes TJR. The finite element method: linear static and dynamic finite element analysis. New Jersey: Prentice Hall; 1987.
[27] Bathe KJ. Finite element procedures. New Jersey: Prentice Hall; 1996.
[28] Carrera E. Theories and finite elements for multilayered, anisotropic, composite plates and shells. Arch Comput Meth Eng 2002;9:1–60.
[29] Hughes TJR, Liu WK. Nonlinear finite element analysis of shells. Part II: Two-dimensional shells. Comput Meth Appl Mech Eng 1981; 27:167–82.
[30] Lam D, Liu WK, Law ES, Belytschko T. Resultant-stress degenerated-shell element. Comput Meth Appl Mech Eng 1986;55:259–300.
[31] Bathe KJ, Dvorkin EN. A formulation of general shell elements—the use of mixed interpolation of tensorial components. Int J Numer Meth Eng 1986;22:697–722.
[32] Simo JC, Fox DD, Rifai MS. On a stress resultant geometrically exact shell model. Part II: The linear theory; computational aspects. Comput Meth Appl Mech Eng 1989;73:53–92.
[33] Heppler GR, Hansen JS. A Mindlin element for thick and deep shells. Comput Meth Appl Mech Eng 1986;54:21–47.
[34] Basar Y, Ding Y, Schultz R. Refined shear-deformation models for composite laminates with finite rotations. Int J Solids Struct 1993;30: 2611–38.